

Kinetic Blume-Capel Model with Random Diluted Single-ion Anisotropy

Gul Gulpinar^{a*}, Erol Vatansever^a

^a*Dokuz Eylül University, Department of Physics, 35160-Buca, İzmir, Turkey*

Abstract

This investigation employs a square lattice and Glauber dynamics methodology to probe the effects of diluteness in the crystal-field interaction in a Blume-Capel Ising system under an oscillating magnetic-field. Fourteen different phase diagrams have been observed in temperature-magnetic-field space as the concentration of the crystal-field interactions is varied. Besides, a comparison is given with the results of the pure spin-1 Ising systems.

Key words: Quenched disorder, Random crystal field, Dynamical critical points, Kinetic Blume-Capel Model.

PACS: 0550, 0570F, 6460H, 7510H

1 Introduction

Ising spin-1 systems, with density as an added degree of freedom, have been utilized to investigate a diverse range of systems: materials with mobile

* corresponding author.

Email address: gul.gulpinar@deu.edu.tr (Gul Gulpinar^a).

defects, structural glasses [1], the superfluid transition in $He^3 - He^4$ mixtures [2], frustrated Ising lattice gas systems [3], binary fluids, binary alloys and frustrated percolation [4]. Recently, Blume-Capel (BC) [6] and Blume-Emery-Griffiths (BEG) models have been used to probe the phenomenon of inverse melting, a phenomena observed in diverse class of systems such as colloids, polymers, miscelles, etc [5].

On the other hand, it is well known that the effects upon criticality and resulting phase diagrams, due to underlying competing interactions in various spin-1 Ising systems can be complicated. Since then, many previous investigations have been focused on various novel types of competing interactions have been the focus of previous studies using the BEG model in conjunction with renormalization-group [7,8,9,10] and/or mean-field methodologies [11,12,13]. Besides, effects of disorder on magnetic systems have been systematically studied, not only for theoretical interests but also for the identifications with experimental realizations [14,15,16]. It has been shown by renormalization group arguments that first-order transitions are replaced by continuous transition, consequently tricritical points and critical end points are depressed in temperature, and a finite amount of disorder will suppress them [17].

An special magnetic system with disorder is spin-1 Ising model with quenched diluted single ion anisotropy is used to model phase separations of superfluidity for helium mixtures in aerogel [18,19]. Due to this fact, various researchers have been motivated to study the effect of the crystal field disorder on the multicritical phase diagram of BC model via effective field theory [20] and mean field approach [21,22], cluster variation method [23], as well as by introducing an external random field [24]. Whereas, Branco et al. considered the effects of random crystal fields using real-space RG [8,9] and mean-field ap-

proximations [9,25] for both BC and BEG model Hamiltonians, respectively. Recently, Snowman has employed a hierarchical lattice and renormalization-group methodology to probe the effects of competing crystal-field interactions in a BC model [26]. Finally, Salmon and Tapia have studied the multicritical behavior of the BC model with infinite-range interactions by introducing quenched disorder in the crystal field Δ_i , which is represented by a superposition of two Gaussian distributions [27].

While the equilibrium properties of the BC model with random single ion anisotropy have been studied extensively, as far as we know, the kinetic aspects of the model have not been investigated via Glauber dynamics. Therefore, the purpose of the present paper is, to present a study of the kinetics of the spin-1 BC model with a quenched two valued random crystal field in the presence of a time-dependent oscillating external magnetic field. We make use of Glauber-type stochastic dynamics to represent the time evolution of the system [28]. More precisely, we have obtained the dynamic phase transition (DPT) points and presented phase diagrams in constant crystal field and the reduced magnetic field amplitude versus reduced temperature plane for various values of the crystal field concentration. This type of calculation for pure BC model, was first performed by Buendia and Machado [29]. They have presented only two phase diagrams in the temperature-magnetic field plane for the pure spin-1 BC model. Later, Keskin et. al. have shown that one of the two phase diagrams in Ref [29] was incomplete; i.e., they had missed a very important part of the phase diagram due to the reason that they did not make the calculations for higher values of the amplitudes of the external oscillating magnetic field [30]. Keskin et. al. presented the phase diagrams in the reduced magnetic field amplitude (h) and reduced temperature (T) plane and calculated five dis-

tinct phase diagram topologies. Recently, Elyadari et.al. has investigated the kinetic Blume Capel Model with a random crystal field distributed according to the following law: $P(\Delta_i) = p\delta(\Delta_i - \Delta(1 + \alpha)) + (1 - p)\delta(\Delta_i - \Delta(1 - \alpha))$. This kind of random crystal field has been introduced to study the critical behavior of ${}^3\text{He} - {}^4\text{He}$ mixtures in random media (aerogel) modeled by the spin-1 Blume-Capel model [31]. In their model, the negative crystal field value corresponds to the field at the pore-grain interface and the positive one is a bulk field that controls the concentration of ${}^3\text{He}$ atoms. In other words, in this kind of randomness the crystal field value is finite for each site about its amplitude takes one of the values $\Delta(1 + \alpha)$ or $\Delta(1 - \alpha)$ with equal and fixed probabilities ($p = 1/2$). While in our current investigation, we have focused on another kind of randomness in which one can see the effect of vacancy of the single-ion anisotropy on the dynamical phase diagrams of the kinetic Blume-Capel model. Previous equilibrium studies has revealed that this kind of randomness leads to a rich variety of phase diagrams with type being according to the concentration p of active local crystal fields. [20,21]. With this motivation we have performed numerical calculations for various values of the crystal field concentrations in order to observe the effect of the quenched vacancy in the crystal field on the five different kinetic phase diagram topologies found by Keskin and co-workers [30].

Meanwhile, it is worthwhile to stress that the DPT was first found in the study of the kinetic Ising system in an oscillating field [32], and it was followed by Monte Carlo simulation researches of kinetic Ising models [33,34]. Further, Tutu and Fujiwara [35] represented a systematic method for obtaining the phase diagrams in DPTs, and constructed a general theory of DPTs near the transition point based on a mean-field description, such as Landau's

general treatment of the equilibrium phase transitions. DPT may also have been observed experimentally in ultrathin Co films on Cu(001) [36] by means of the surface magneto-optic Kerr effect and in ferroic systems (ferromagnets, ferroelectrics and ferroelastics) with pinned domain walls [39] and ultra-thin $[Co/Pt]_3$ multilayer [37]. In addition, reviews of earlier research on the DPT and related phenomena are found in Ref [34].

The paper is organized as follows: In Sec.2, we discuss the kinetic BC model with single ion isotropy briefly. Moreover, the derivation of the mean-field dynamic equations of motion is given by using a master equation formalism in the presence of an oscillating external magnetic field is also given in Sec.2. In Sec.3, the DPT points are calculated and the phase diagrams presented. Finally, Sec.4 represents the summary and conclusions.

2 DYNAMICAL EQUATIONS FOR THE MEAN VALUES

The generalization of the kinetic BC model for a quenched random crystal field is given by the Hamiltonian,

$$\hat{H} = -J \sum_{\langle ij \rangle} S_i S_j - \sum_{\{i\}} \Delta_i S_i^2 - H \sum_{\{i\}} S_i , \quad (1)$$

where the spin variables $S_i = 0, \pm 1$ on a square lattice. The first and the second sums are over nearest neighbor pairs. The exchange interaction with strength $J > 0$ is responsible for the ferromagnetic ordering, while the random single ion anisotropy Δ_i is given by the following joint probability density:

$$P(\Delta_i) = p\delta(\Delta_i - \Delta) + (1 - p)\delta(\Delta_i) . \quad (2)$$

Finally, H is a time-dependent external oscillating magnetic field and given by,

$$H(t) = H_0 \cos(\omega t) , \quad (3)$$

here H_0 and $\omega = 2\pi\nu$ denote the amplitude and the angular frequency of the oscillating field respectively.

When we put this system in contact with a heat reservoir at temperature T , the spin variables S_i can be considered as stochastic functions of time. The system evolves according to a Glauber-type stochastic process at a rate of $\frac{1}{\tau}$ transitions per unit time. More precisely, we will follow the heat-bath prescription [38]: the new value of the spin variable at site i ($S_{i\ new}$) is determined by testing all its possible states in the heat-bath of its (fixed) neighbors (here four on a square lattice):

$$w_i(S_{i\ old} \rightarrow S_{i\ new}) = \frac{1}{\tau} \frac{\exp\{-\beta\Delta E(S_{i\ old} \rightarrow S_{i\ new})\}}{\sum \exp\{-\beta\Delta E(S_{i\ old} \rightarrow S_{i\ new})\}} , \quad (4)$$

where $\beta = \frac{1}{kT}$ and τ defines a time scale (characteristic mean time interval for one spin flip), and

$$\Delta E(S_{i\ old} \rightarrow S_{i\ new}) = (S_{i\ old} - S_{i\ new}) \left(J \sum_{\langle j \rangle} S_j + H \right) - (S_{i\ old}^2 - S_{i\ new}^2) \Delta_i , \quad (5)$$

give the changes in the energy of the system in the case of flipping of the i^{th} spin in the lattice. If we define $P(S_1, S_2, \dots, S_N; t)$ as the probability that the system has the configuration $\{S_1, S_2, \dots, S_N\}$, at time t . Making use of master equation formalism [28], one can write the time derivative of $P(S_1, S_2, \dots, S_N; t)$

as,

$$\begin{aligned} \frac{d}{dt}P(S_1, \dots, S_N; t) = & - \sum_i \sum_{S_{i \text{ old}} \neq S_{i \text{ new}}} w_i(S_{i \text{ old}} \rightarrow S_{i \text{ new}})P(S_1, \dots, S_{i \text{ old}}, \dots, S_N; t) \\ & + \sum_i \sum_{S_{i \text{ old}} \neq S_{i \text{ new}}} w_i(S_{i \text{ new}} \rightarrow S_{i \text{ old}})P(S_1, \dots, S_{i \text{ new}}, \dots, S_N; t) . \end{aligned} \quad (6)$$

The detailed balance condition reads,

$$\frac{w_i(S_{i \text{ old}} \rightarrow S_{i \text{ new}})}{w_i(S_{i \text{ new}} \rightarrow S_{i \text{ old}})} = \frac{P(S_1, S_2, \dots, S_{i \text{ new}}, \dots, S_N)}{P(S_1, S_2, \dots, S_{i \text{ old}}, \dots, S_N)} . \quad (7)$$

In addition, substituting the possible values of $S_{i \text{ new}}$ and $S_{i \text{ old}}$, one obtains:

$$\begin{aligned} w_i(1 \rightarrow 0) = w_i(-1 \rightarrow 0) &= \frac{1}{\tau} \frac{\exp(-\beta\Delta_i)}{2\cosh(\beta\delta) + \exp(-\beta\Delta_i)} , \\ w_i(1 \rightarrow -1) = w_i(0 \rightarrow -1) &= \frac{1}{\tau} \frac{\exp(-\beta\delta)}{2\cosh(\beta\delta) + \exp(-\beta\Delta_i)} , \\ w_i(0 \rightarrow 1) = w_i(-1 \rightarrow 1) &= \frac{1}{\tau} \frac{\exp(\beta\delta)}{2\cosh(\beta\delta) + \exp(-\beta\Delta_i)} , \end{aligned} \quad (8)$$

where $\delta = J \sum_{\langle j \rangle} S_j + H$. At this point one can notice that $w_i(S_{i \text{ old}} \rightarrow S_{i \text{ new}})$ does not depend on the value $S_{i \text{ old}}$, we can write $w_i(S_{i \text{ old}} \rightarrow S_{i \text{ new}}) = w_i(S_{i \text{ new}})$, then the master equation becomes:

$$\begin{aligned} \frac{d}{dt}P(S_1, \dots, S_N; t) = & - \sum_i \sum_{S_{i \text{ old}} \neq S_{i \text{ new}}} w_i(S_{i \text{ new}})P(S_1, \dots, S_{i \text{ old}}, \dots, S_N; t) \\ & + \sum_i w_i(S_{i \text{ old}}) \sum_{S_{i \text{ old}} \neq S_{i \text{ new}}} P(S_1, \dots, S_{i \text{ new}}, \dots, S_N; t) . \end{aligned} \quad (9)$$

On the other hand, the sum of probabilities is normalized to one so that by multiplying both sides of Eq.(9) by S_p and taking the average, one obtains,

$$\tau \frac{d}{dt} \langle S_p \rangle = - \langle S_p \rangle + \left\langle \int P(\Delta_i) \frac{2 \sinh \left(\beta \left[J \sum_{\langle j \rangle} S_j + H \right] \right)}{2 \cosh \left(\beta \left[J \sum_{\langle j \rangle} S_j + H \right] \right) + \exp(-\beta \Delta_i)} d\Delta_i \right\rangle . \quad (10)$$

Finally, after integration over the distribution of $P(\Delta_i)$ and making use of mean field approximation, the kinetic equation of the magnetization becomes,

$$\Omega \frac{d}{d\xi} m = -m + p \frac{2\sinh(\frac{m+h\cos(\xi)}{T})}{2\cosh(\frac{m+h\cos(\xi)}{T}) + \exp(-\frac{d}{T})} + (1-p) \frac{2\sinh(\frac{m+h\cos(\xi)}{T})}{2\cosh(\frac{m+h\cos(\xi)}{T}) + 1}, \quad (11)$$

where $\xi = \omega t$, $m = \langle S \rangle$, $T = (\beta z J)^{-1}$, $d = \Delta/zJ$, $h = H_0/zJ$. In these equations the variable Ω was defined as the ratio between the external field frequency ω and the frequency of spin flipping ($f = 1/\tau$), i.e., $\Omega = \omega\tau = \omega/f$. Here we consider a cooperatively interacting many-body system, driven by an oscillating external perturbation, an oscillating magnetic field so that the thermodynamic response of the system, the magnetization, will then also oscillate with necessary modifications in its form [34]. Moreover, the time dependence of magnetization can be one of two types according to whether they have or do not have the property:

$$m(\xi + \pi) = -m(\xi). \quad (12)$$

A solution that satisfies Eq.(12) is called symmetric solution; it corresponds to a paramagnetic (P) phase. In this solution, the magnetization $m(\zeta)$ oscillates around the zero value and is delayed with respect to the external field. Solutions of the second type, which do not satisfy Eq.(12), are called non-symmetric solutions; they correspond to a ferromagnetic (F) phase. In this case, the magnetization does not follow the external magnetic field any more, but, instead, oscillates around a nonzero value. Eq. (11) is solved numerically by using fourth order Runge-Kutta method for fixed values of T, d, p , and Ω . Throughout this study we have fixed $\Omega = 2\pi$, $J = 1$ and $z = 4$ for a given set of parameters and initial values. The results are presented in Figs.1(a)-(c). Here, we can see three different solutions: F,P and coexistence of F and P (F+P).

In Fig.1(a), only the symmetric solution is always obtained, and, hence, we have a paramagnetic (P) solution; but, in Fig.1(b), only the nonsymmetric solutions are found, and we, therefore, have a ferromagnetic (F) solution. One can observe from these figures that these solutions do not depend on the initial values. On the other hand, in Fig.1(c), both the F and P phases exist in the system this case corresponds to the coexistence solution (F + P). As can be seen in Fig.1(c) explicitly, the solutions depend on the initial values.

3 DYNAMIC PHASE TRANSITION POINTS AND PHASE DIAGRAMS

In order to obtain the dynamic phase boundaries between three phases or regions in that are given Figs.1(a)-(c), one should calculate the DPT points. The DPT points are obtained by investigating the behavior of the average magnetization in a period as a function of the reduced temperature.

$$M = \frac{1}{2\pi} \int_{\xi_0}^{\xi_0+2\pi} m(\xi) d\xi, \quad (13)$$

Here $m(\xi)$ is a stable and periodical function. In general our solution stabilizes after 6000 periods. In this manner, ξ_0 can take any value after this transient. In the high field and high temperature region time dependent staggered magnetization follows the reduced external magnetic field within a single period which corresponds to vanishing time average of the dynamical order parameter (paramagnetic phase). Whereas, at low field values the magnetization can not fully switch sign in a single period and the time average of the magnetization in a period is non zero and consequently ordered or ferro-

magnetic phase arises. Fig.2 represents the reduced temperature dependence of the average magnetization (M) for various values of magnetic field amplitude h and crystal field concentration (p) while $d = -0.25$. In these figures arrows denote the transition temperatures. In Fig.2(a), we give the case for $h = 0.70, p = 0.50$. In this case, the system represents re-entrance with two sequential first order phase transitions which take place at T_{t1} and T_{t2} . While Fig.2(b) exhibits the reduced temperature dependence of the dynamical order parameter for $h = 0.70, p = 0.75$. For these values of the parameters, BC model with random single ion anisotropy undergoes a first and a second phase transition sequentially. In Fig.2(c) we give an example of second order phase transition from ordered to disordered phase for $h = 0.4, p = 0.75$. Eventually, Fig.2(c) illustrates an first order phase transition which occurs for $h = 0.75, p = 0.75$.

Fig.3(a) illustrates the thermal variations of M for various values of crystal field concentration (p) for vanishing external field. The number accompanying each curve illustrates the value of p . Here the crystal field has negative sign ($d = -0.3$) since then the critical temperature increases with increasing diluteness for fixed h .

On the other hand, it is well known fact that in the static limit ($\omega = 0.0$) the dynamic transition disappears and the phase boundary in the $h - T$ plane collapses to a line with $h = 0$ and ending at $T = T_c$, the static transition temperature of the unperturbed system [34]. Fig.3(b) shows the thermal variations of M and for several values of static h while $d = -0.5$. In addition, Fig.3(c) gives the behaviors of M and as a function of static h for $d = -0.5$ and several values of T . One can see from these figures that the system does not undergo any phase transitions for static h . Consequently, we can conclude

that the oscillating external magnetic field induces the phase transitions.

We can now focus on the phase diagrams of the system. In Figs.3-5 we represent the calculated mean field dynamical phase diagrams in the (T,h) plane which exhibit the effect of the randomness in the crystal field on the five different phase diagram topologies of the pure kinetic BC model [30]. First in Fig.3(a), we give the dynamical phase diagram of the two-dimensional kinetic BC model with bimodal crystal field distribution for $d = 0.25$. The number accompanying each curve denotes the value of the crystal field concentration (p). The outermost curve corresponds to the pure BC model with no quenched randomness ($p = 0$). As crystal field quenched randomness is introduced with decreasing values of p , ordered phases and first-order phase transitions recede. This result is consistent with the RG theory predictions given in Ref.[17]. Finally, we should stress that similar phase diagrams were also obtained in the kinetic of the mixed spin- $\frac{1}{2}$ and spin-1 Ising ferromagnetic system [29] as well as the kinetic spin- $\frac{1}{2}$ Ising model [32]. The reason that the phase diagram is similar to the one obtained for the kinetic spin- $\frac{1}{2}$ Ising model is due to the competition between J, d and h . For positive crystal field values, the Hamiltonian of the spin-1 model gives similar results to the Hamiltonian of the spin- $\frac{1}{2}$ Ising model.

It has been given in Ref.[30] that pure kinetic BC model has four different phase diagram topologies for negative d , which depend on d values. Now let us discuss the effect of randomness in the single ion isotropy on these phase diagrams:

(1) For $-0.0104 > d \geq -0.4654$, the dynamical phase diagram topology of the pure kinetic BC model is similar to positive d case but only differs in that for very low T and h values, one more P+F coexistence region also exists.

The boundary between this F+P region and the F phase is the first-order line (see Fig.7(b) in Ref.[30]. In BC model, described by the Hamiltonian given in Eq.(1), negative crystal field interaction ($d = \Delta/zJ < 0$) favors the annealed vacancies, namely the nonmagnetic states $S_i = 0$. Fig.3(b) exhibits this fact: with increasing concentration of negative single ion isotropy ($d = -0.25$) the ordered phase recedes and the tricritical temperature moves to lower temperatures. Whereas, the coexistence region (F+P) in the low temperature and field region disappears with increasing vacancy in the single ion anisotropy (for $p \leq 0.95$).

(2) For $-0.4654 < d \leq -0.5543$, the system exhibits two dynamic tricritical points (DTCP). One of them occurs in similar places in the phase diagrams for $d = 0.25$ and $d = -0.25$, whereas, the other DTCP occurs in the low h region. In addition, the first-order phase transition lines exist at the low reduced temperatures, and h values separate not only the P+F region from the F phase, but also from the P phase. When we introduce quench disorder in the crystal field we found that this topology changes drastically with varying crystal field concentration (p). Our calculations has revealed that there are four different phase diagram topologies which depend on p values:

(2.a) Type 1 ($p \geq 0.97$): the system has the same phase diagram with the pure case (see Fig.3(c)).

(2.b) Type 2 ($0.97 > p \geq 0.85$): The DTCP in the low temperature and field region disappears. Whereas, the second order line intersects the $h = 0$ axis. Moreover, the P+F phase recedes and an ordered phase appears in the neighborhood of $h = 0, T = 0$ (see Fig.3(d)).

(2.c) Type 3 ($0.85 > p \geq 0.31$): with increasing single ion isotropy vacancy, the coexistence region in the low H and low T region moves to higher

field values (see Fig.3(e)). The diagram contains one DTCP first-order phase transition lines merge and signals the change from a first- to a second-order phase transitions.

(2.d) Type 4 ($0.31 > p \geq 0.0$): Now the crystal field interaction is rather diluted. As one can see from Fig.3(f) that the F+P phase coexistence totally disappears and the phase diagram is similar to the $-0.0104 > d \geq -0.4654$ case.

(3) For $-0.5543 < d \leq -0.9891$, pure system exhibits an exotic phase diagram which contains, three different the F+P regions at low reduced temperatures in addition to the P and F phases and two dynamical tricritical points. On the other hand, if one introduces disorder in the crystal field there are four different phase diagram topologies which depend on the concentration of the crystal field (see Figs.5(a)-(d).):

(3.a) Type 1 ($1.0 \geq p > 0.8$): Although the dynamical phase diagram of the random single ion-anisotropy BC model has similar topology with the pure kinetic spin-1 BC model, one can observe that (see Fig.7(d) of Ref.[30]) the ordered phase moves to lower temperatures and the coexistence region in the low temperature and field region shrinks with raising amount of the crystal field randomness and finally disappears at $p=0.79$.

(3.b) Type 2 ($0.80 \geq p > 0.32$): For this interval of the crystal field concentration, the ferromagnetic phase expands in the expense of the F+P and P phases and due to this effect the first order transition line which takes place in the high field low temperature regime disappears and the system has only one DTCP.

(3.c) Type 3 ($0.32 \geq p > 0.1$): The phase boundary that separates F+P coexistence phases and F phase turns out to be second order as consequence

the dynamical TCP moves to zero temperature . Whereas, the boundary between F+P and P phases remains as first order. In addition to the DTCP, system exhibits a dynamical critical end point (DCEP) which is shown Fig. (5.c)

(3.d) Type 4 ($0.1 \geq p \geq 0.0$): The behavior differs from Type 3 in the sense that for very low T and h values, P+F coexistence region disappears and system represents no DCEP. For this interval of the concentration value, the system has only one DTCP which exists at low temperature and high magnetic field.

(4) For $-0.9891 > d$, the topology of the phase diagram is dramatically different from the other intervals of the single ion anisotropy amplitude : it does not include a P+F phase coexistence region at low temperature and low magnetic field for pure spin-1 BC model. In Figs. 6(a) to (d) we illustrate the four different types of behavior depending on the the p:

4(a) Type 1 ($1 \geq p > 0.994$): For this interval of the crystal field amplitude, the system exhibits two DTCP's and the topology of the phase diagram is very similar to the pure case.

4(b) Type 2 ($0.993 \geq p > 0.14$): The phase boundary that separates F+P coexistence phases and F phase turns to be second order line with decreasing concentration value of the randomness single-ion anisotropy. As a result of this, the undermost DTCP turns out to be a DCEP.

4(c) Type 3 ($0.14 \geq p \geq 0$): Finally, for $d=-1$ and $p=0$, the system exists one DTCP at low temperature and high magnetic field. The point where the two boundary lines merge. Also this behavior is similar to kinetic mixed Ising [29] and kinetic spin-1/2 Ising model [32].

4 SUMMARY AND CONCLUSIONS

Within the mean field approach, we have analyzed stationary states of the spin-1 Blume-Capel model with a random crystal field Δ_i under a time-dependent oscillating external magnetic field. The time evolution of the system is described by a stochastic dynamics of the Glauber type. We have studied the time dependence of the magnetization and the behavior of the dynamical order parameter as a function of reduced temperature for reduced magnetic field and different possibility (p) of the crystal field. We have also analyzed thermal variations and temperature dependence of M for various values of crystal field concentration (p) and for different static reduced magnetic field, respectively. Moreover, the behavior of M as function of static reduced magnetic field (h) for various values of the reduced temperature have been examined.

The dynamic phase transition (DPT) points are found and the phase diagrams are constructed in the reduced magnetic field and temperature plane. We have found that the behavior of the system strongly depends on the values of random crystal field or random single-ion anisotropy. For all (p) and positive values of reduced crystal field (d) the system behaves as the standard kinetic Ising model [32], and also kinetic mixed Ising spin-(1/2,1) model [29]. We have observed that there exist F+P coexistence and first order dynamical phase transitions in the low temperature and high field regime. Whereas, the dynamical phase transitions turns out to be second order with increasing temperature and decreasing magnetic field. Consequently, it shows that the system exhibits dynamical tricritical point (DTCP). As we have mentioned in detail in the previous section, the introduction of random ion-anisotropy in kinetic spin-1 BC model produces an effect which suppress the F+P coexistence region

in the low temperature low field and high field low temperature regimes. We should stress that this result is in accordance with the previous results obtained by Renormalization-Group theory [17]. Finally we should point out that some of the first-order phase lines and also the dynamic multicritical points (DTCP and DCEP) are very likely artifacts of the mean-field approach. The reason of this artifact can be stated as follows: for field amplitudes less than the coercive field and temperatures lower than the static ferromagnetic - paramagnetic transition temperature, the time dependent magnetization represents a nonsymmetric stationary solution even in the zero frequency limit. Meanwhile in the absence of the fluctuations, the system is trapped in one well of the free energy and cannot go to other one [33]. On the other hand, this mean-field dynamic study reveals that the random single ion anisotropy spin 1 Blume-Capel Model represents interesting dynamic phase diagram topologies. Since then, we hope that this work can stimulate further studies on kinetic features of kinetic random single ion anisotropy spin-1 Model systems theoretically and experimentally.

5 ACKNOWLEDGMENTS

This research was supported by the Scientific and Technological Research Council of Turkey (TUBITAK), including computational support through the TR-Grid e-Infrastructure Project hosted by ULAKBIM, and by the Academy of Sciences of Turkey.

References

- [1] Kirkpatrick T R and Thirumalai D 1987 Phys. Rev. B 36 5388.
- [2] Blume M, Emery V J and Griffiths R B 1971 Phys. Rev. A 4 1071.
- [3] Nicodemi M and Coniglio A 1997 J. Phys. A 30 L187.
Arenzon J J, Nicodemi M and Sellitto M 1996 J. Phys. I 6 1143.
- [4] Coniglio A 1993 J. Phys. IV 3 C1-1 .
- [5] Schupper N and Shnerb N M 2005 Phys. Rev. E 72 046107.
Angelini R, Ruocco G and Panfilis S De 2008 Phys. Rev. E 78 020502.
- [6] Blume M 1966 Phys. Rev. 141 517.
Capel H W 1966 Physica 32, 966 .
- [7] Berker A N and Wortis M 1976 Phys. Rev. B 14 4946.
McKay S R, Berker A N, and Kirkpatrick S 1982 Phys. Rev. Lett. 48 767.
- [8] Branco N S and Boechat B M 1997 Phys. Rev. B 56 11673.
- [9] Branco N S 1999 Phys. Rev. B 60 1033.
- [10] Snowman D P 2007 J. Magn. Magn. Mater. 314 69.
Snowman D P 2008 J. Magn. Magn. Mater. 320 1622.
Snowman D P 2008 Phys. Rev. E 77 041112.
- [11] McKay S R and Berker A N 1984 J. Appl. Phys. 55 1646.
- [12] Hoston W and Berker A N 1991 Phys. Rev. Lett. 67 1027.
- [13] Sellitto M, Nicodemi M, and Arenzon J J 1997 J. Phys. I 7 945.
- [14] Bouchiat H, Dartyge E, Monod P and Lambert M 1981 Phys. Rev. B 23 1375.
- [15] Katsumata K, Nire T and Tanimoto M 1982 Phys. Rev. B 25 428.

- [16] For an experimental review, see Belanger D P and Young A P 1991 J. Magn. Mater. 100 272.
- [17] Hui K, Berker A N 1989 Phys. Rev. Lett. 62 2507.
Falicov A and Berker A N 1996 Phys. Rev. Lett. 76 4380.
Ozcelik V O and Berker A N 2008 Phys. Rev. E 78 031104.
- [18] Maritan A, Cieplak M, Swift M R , Toigo F and Banavar J R 1992 Phys. Rev. Lett. 69 221.
- [19] Buzano C, Maritan A, Pelizzola A 1994 J. Phys. Condens. Matter 6 327.
- [20] Kaneyoshi T 1986 J. Phys. C: Solid State Phys. 19 L557.
- [21] Benyoussef A, Biaz T, Saber M and Touzani M 1987 J. Phys. C: Solid State Phys. 20 5349.
- [22] Boccara N, Elkenzi A and Sabers M 1989 J. Phys.: Condens. Matter 1 5721.
Carneiro C E I, Henriques V B and Salinas S R 1989 J. Phys.: Condens. Matter 1 3687.
Carneiro C E I, Henriques V B and Salinas S R 1990 J. Phys. A: Math. Gen. 23 3383.
Ez-Zahraouy H and Kassou-Ou-Ali A 2004 Phys. Rev. B 69 064415.
- [23] Buzano C, Maritan A and Pelizzola A 1994 J. Phys. Condensed Matter. 6 327.
- [24] Kaufman M and Kanner M 1990 Phys. Rev. B 42 23.
- [25] Branco N S and Bachmann L 1998 Physica A 257 319.
- [26] Snowman D P 2009 Phys. Rev. E 79 041126.
- [27] Salmon O D R and Tapia J R 2010 J. Phys. A: Math. Theor. 43 125003.
- [28] Glauber R J 1963 J. Math. Phys. 4 294.
- [29] Buendia G M and Machado E 1998 Phys. Rev. E 58 1260.

- [30] Keskin M, Canko O and Temizer U 2005 Phys. Rev. E 72 036125.
- [31] El Yadari M, Benayad M R, Benyoussef A, and El Kenz A 2010 Physica A, 389 4677.
- [32] Tome T and de Oliveira M J 1990 Phys. Rev. A 41 4251.
- [33] Acharyya M 1997 Phys. Rev. E 56 2407.
Chatterjee A and Chakrabarti B K 2003 *ibid.* 67 046113.
Sides S W, Rikvold P A, and Novotny M A 1998 Phys. Rev. Lett. 81 834.
Sides S W, Rikvold P A, and Novotny M A 1999 Phys. Rev. E 59 2710.
Korniss G, White C J, Rikvold P A, and Novotny M A 2000 *ibid.* 63 016120.
Korniss G, Rikvold P A, and Novotny M A 2002 *ibid.* 66 056127.
- [34] Chakrabarti B K and Acharyya M 1999 Rev. Mod. Phys. 71 847.
- [35] Tutu H and Fujiwara N 2004 J. Phys. Soc. Jpn. 73 2680.
- [36] Jiang Q, Yang H N, and Wang G C 1995 Phys. Rev. B 52 14911.
Jiang Q, Yang H N, and Wang G C 1996 J. Appl. Phys. 79 5122.
- [37] Robb D T, Xu Y H, Hellwig O, McCord J, Berger A, Novotny M A, and Rikvold P A 2008 Phys. Rev. B 78 134422.
- [38] Janke W Computer Simulations in Condensed Matter Physics, Vol. VII, ed. by Landau D, Mon K, Schuttler H B Berlin, 1994 Springer .
- [39] Kleemann W, Braun T, Dec J, and Petravic O 2005 Phase Transit. 78 811.

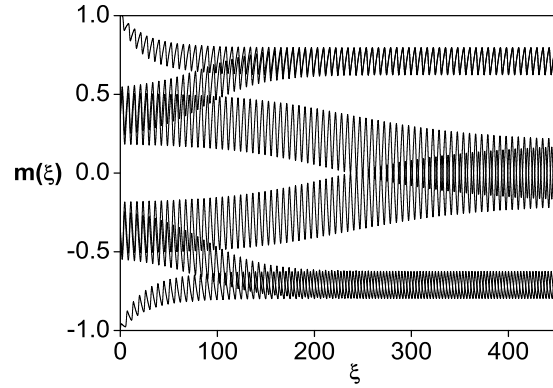
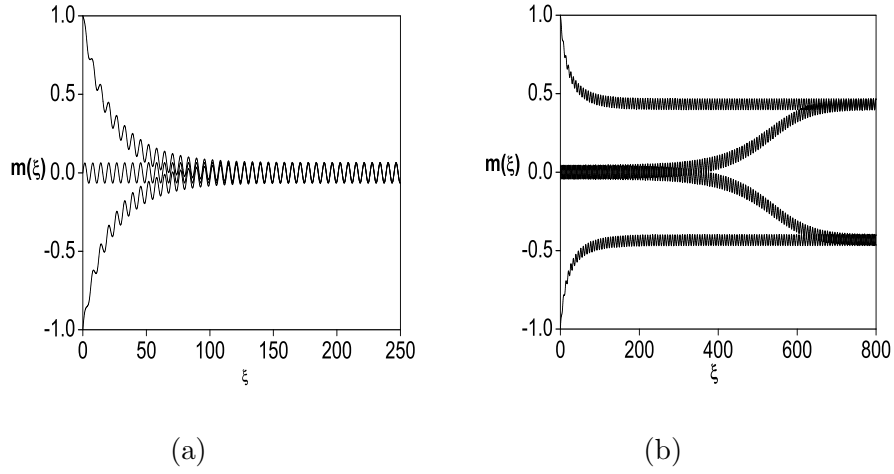


Fig. 1. Time variance of the magnetization ($m(\xi)$) while $p=0.9$: (a) Corresponding to a paramagnetic phase (P) for $d=-0.25$, $h=0.5$, and $T=0.7$; (b) Exhibiting a ferromagnetic phase (F) for $d=-0.25$, $h=0.25$, and $T=0.5$; (c) Representing a coexistence region (F+P) $d=-0.25$, $h=0.75$, and $T = 0.1$.

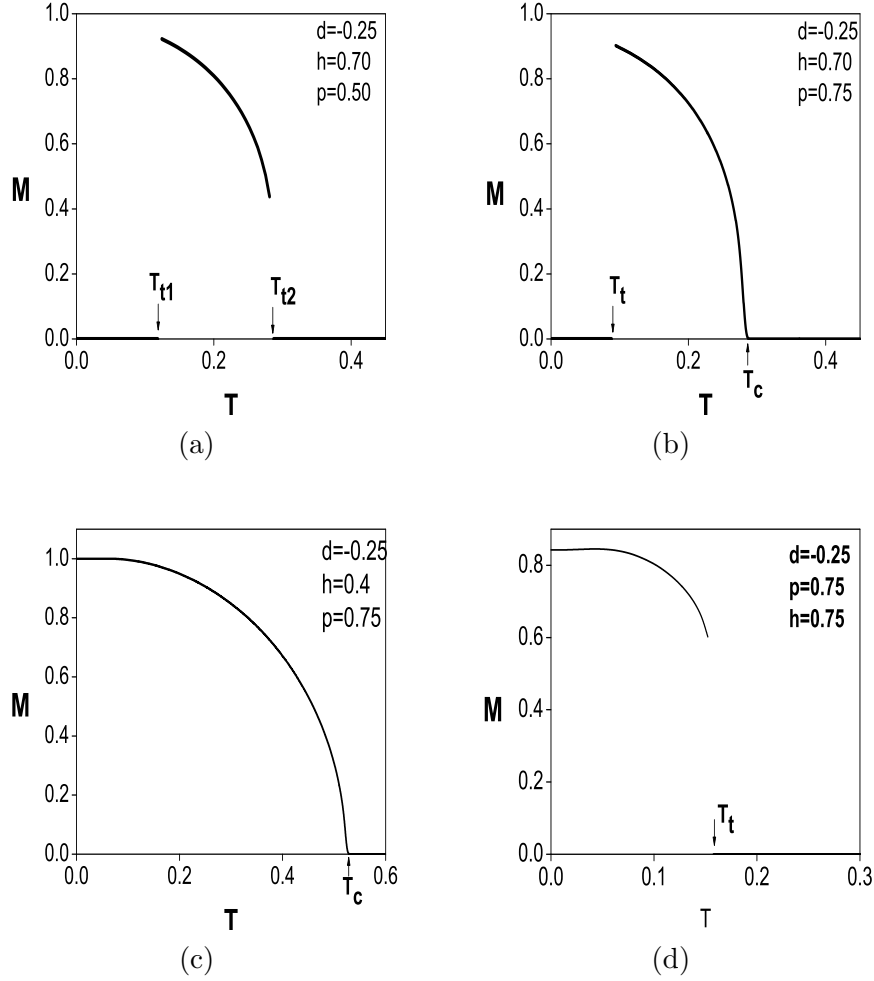


Fig. 2. Dynamical order parameter as a function of reduced temperature. T_c and T_t indicate second and first order phase transition temperatures respectively. (a) The system under goes two successive first order phase transitions, there exists re-entrance. (b) Two successive phase transitions: the first one is a first-order and the second one a continuous phase transition and there is re-entrance. (c) The system under goes a second order phase transition. (d) The system shows a first order phase transition.

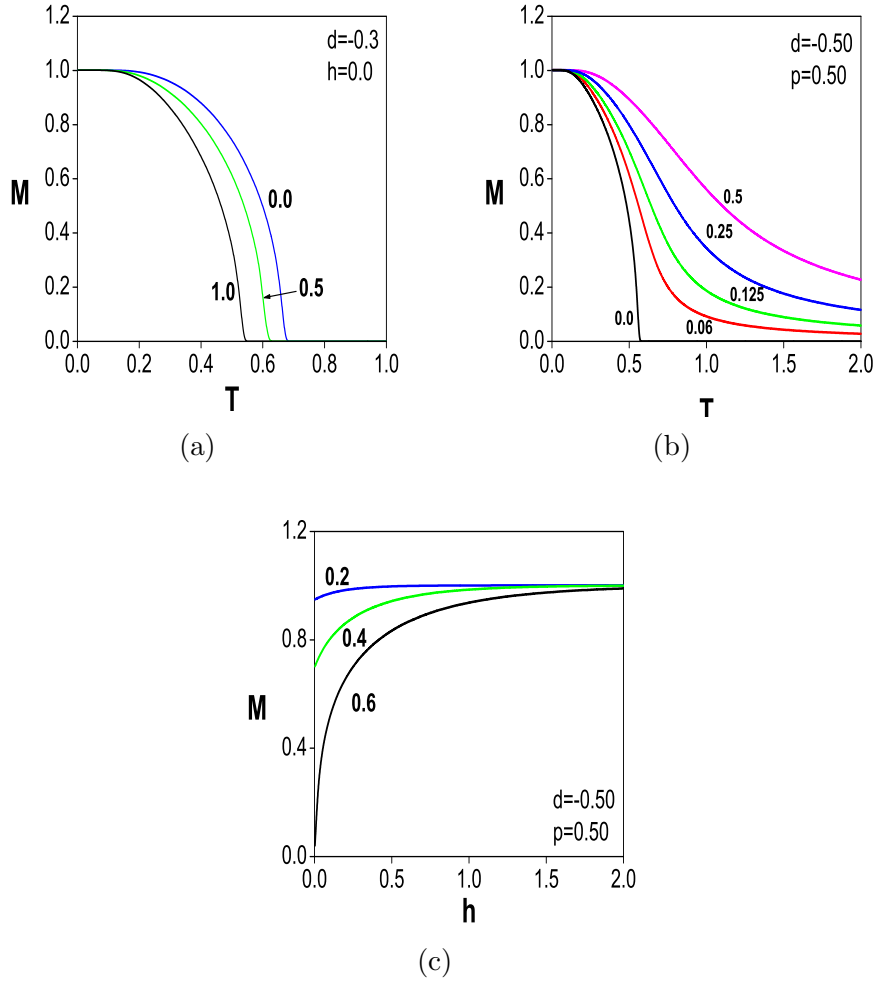


Fig. 3. (a) Thermal variations of M for various values of crystal field concentration (p) for vanishing external field. The number accompanying each curve illustrates the value of p . (b) Temperature dependence of M for several values of static external field amplitudes (h) while $p = 0.5$. The number accompanying each curve denotes the value of h . (c) The behavior of M as function of static h for $d = -0.5$. The number accompanying each curve denotes the value of the reduced temperature (T).

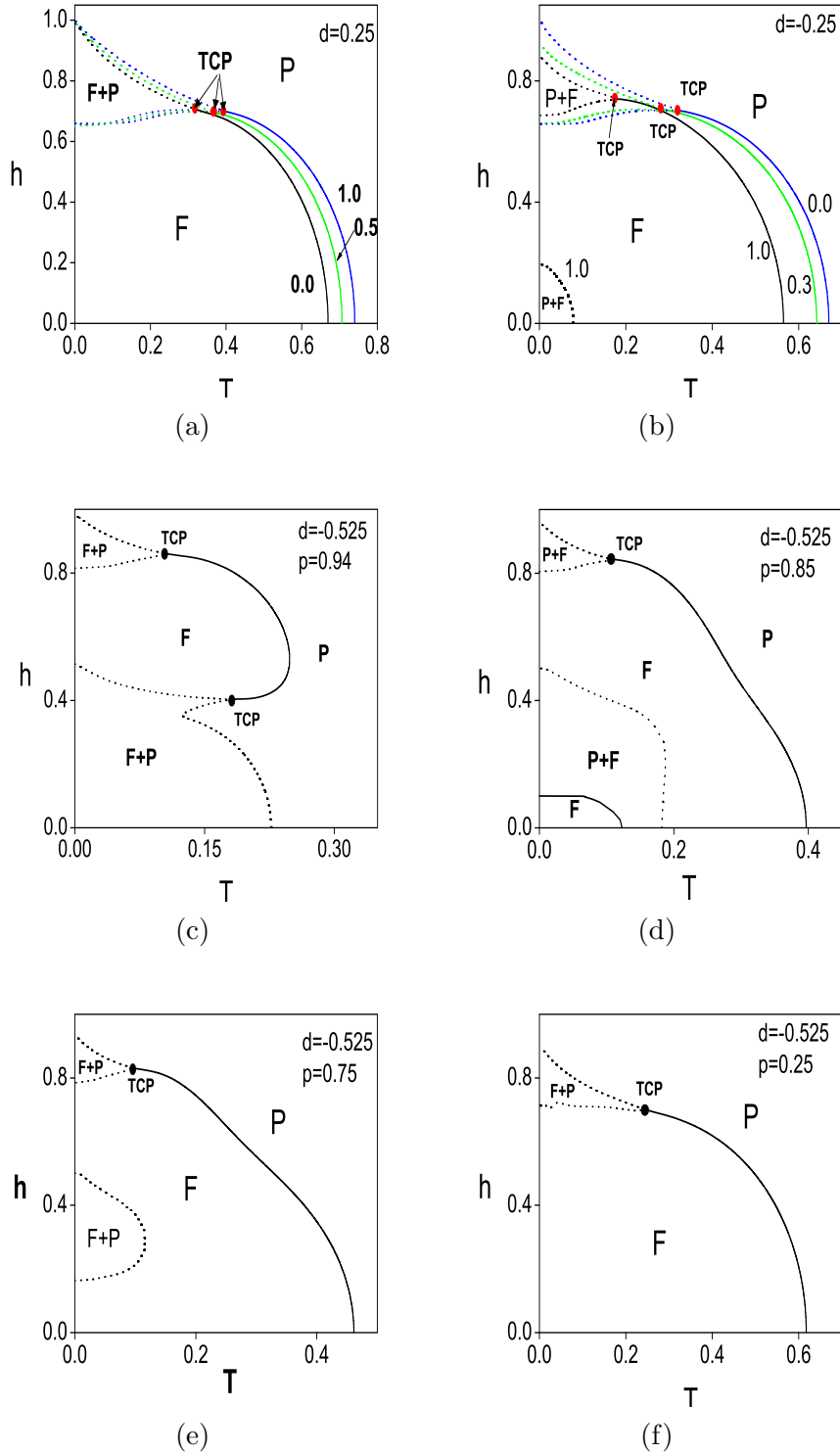


Fig. 4. Dynamic phase diagrams of the Blume-Capel model with crystal field randomness in the (T, h) plane for various values of the single ion anisotropy concentration (p). Dotted and solid lines represent the first-order and second-order phase transitions, respectively. (a) $d=0.25$, the number accompanying each curve denotes the value of p . (b) $d=-0.25$ the number accompanying each curve illustrates the value of p . (c) $d=-0.525$ and $p=0.94$. (d) $d=-0.525$ and $p=0.85$. (e) $d=-0.525$ and $p=0.75$. (f) $d=-0.525$ and $p=0.25$.

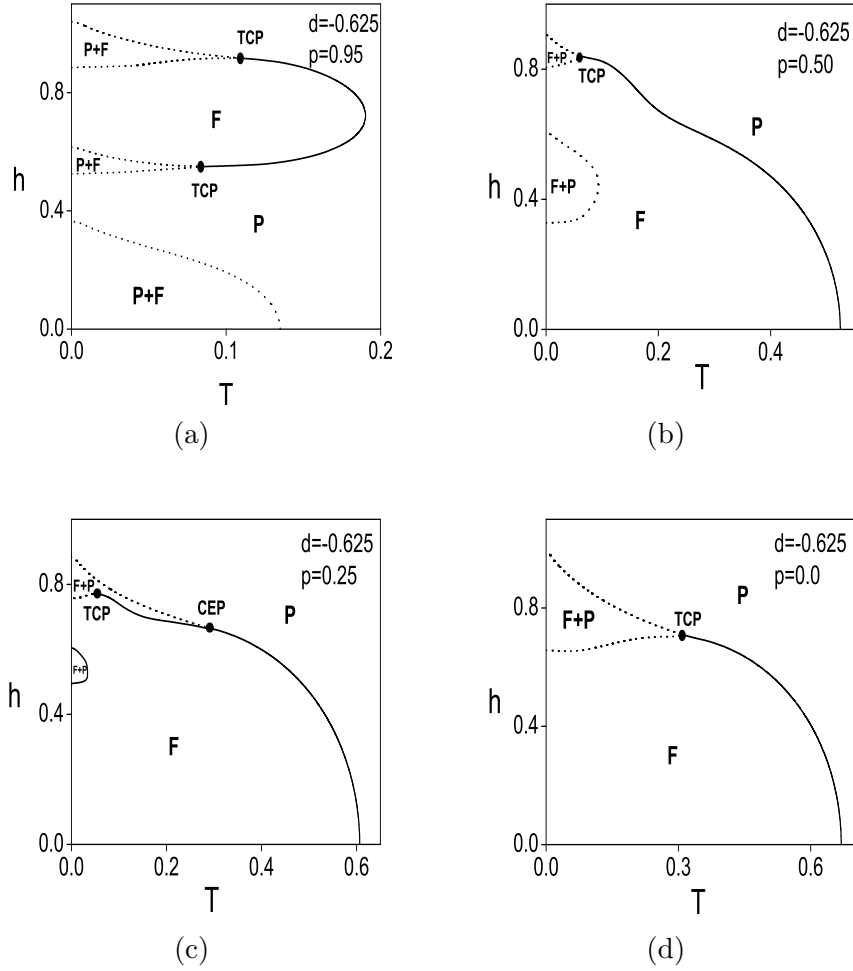


Fig. 5. Dynamic phase diagrams of the Blume-Capel model with crystal field randomness in the (T, h) plane for various values of the single ion anisotropy concentration (p) while $d=-0.625$. Dotted and solid lines represent the first-order and second-order phase transitions, respectively. (a) $p=0.95$, (b) $p=0.50$, (c) $p=0.25$, (d) $p=0.0$.

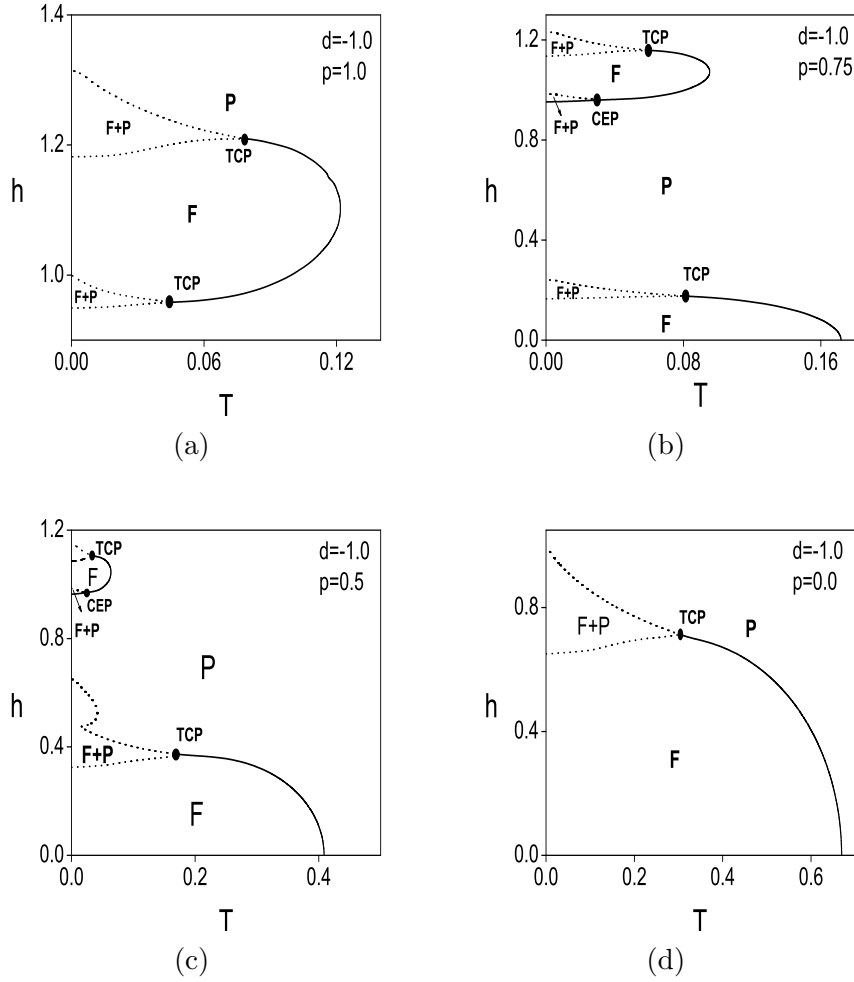


Fig. 6. Dynamic phase diagrams of the Blume-Capel model with crystal field randomness in the (T, h) plane for different values of the single ion anisotropy concentration (p) while $d = -1.0$. Dotted and solid lines represent the first-order and second-order phase transitions, respectively. (a) $p = 1.0$, (b) $p = 0.75$, (c) $p = 0.5$, (d) $p = 0.0$.